GSC Biological and Pharmaceutical Sciences
eISSN: 2581-3250 CODEN (USA): GBPSC2
Cross Ref DOI: 10.30574/gscbps
Journal homepage: https://gsconlinepress.com/journals/gscbps/

(RESEARCH ARTICLE)

Check for updates

Vanillin Esterified TEMPO-Oxidised Nanocellulose Derived from Sugarcane Bagasse for Antibacterial Applications

Guruprasad R. Mavlankar [1], Akshay Chavan [1], Prajakta P. Baikar [1], Deepa N. Rangadal [1], Minakshi N. Bhatu[1, 2] and Shubhangi P. Patil [1, *]

[1] *The Institute of Science, 15, Madam Cama Road, Mantralaya, Fort, Mumbai, Maharashtra 400032, India*
[2] *Annasaheb Vartak College of Arts, Kedarnath Malhotra College of Commerce, E. S. Andrades College of Science, Vasai Road (West), Maharashtra 401 202, India.*

GSC Biological and Pharmaceutical Sciences, 2025, 33(03), 361-375

Publication history: Received on 17 November 2025; revised on 25 December 2025; accepted on 27 December 2025

Article DOI: https://doi.org/10.30574/gscbps.2025.33.3.0526

Abstract

Nanocellulose extracted from sugarcane bagasse underwent chemical modification. Then 2,2,6,6-Tetramethylpiperidin-1-yl)oxyl (TEMPO) -mediated oxidation followed by esterification with vanillin, resulting in the development of a novel antibacterial material. The sequential processes of alkali treatment, bleaching, and acid hydrolysis effectively eliminated non-cellulosic components, producing purified cellulose nanofibers with enhanced crystallinity (88%) and well-defined morphology, as confirmed by Fourier transform infrared spectroscopy (FTIR), X-ray diffraction (XRD), scanning electron microscopy (SEM), and Transmission electron microscopy (TEM) analyses. TEMPO oxidation selectively converted primary C6 hydroxyl groups to carboxylic acids, as evidenced by FTIR and solid-state ^{13}C nuclear magnetic resonance (^{13}C SS-NMR) spectroscopy. The esterification of the oxidised nanocellulose with vanillin was accomplished using FTIR spectra, ^{13}C SS-NMR. The vanillin-functionalized nanocellulose exhibited reduced thermal stability checked by thermogravimetric analysis (TGA). Notably, the modified nanocellulose demonstrated significant antibacterial activity against both Gram-positive and Gram-negative bacteria, with inhibition zones 20.33 to 21.66 mm comparable to those of pure vanillin, indicating the retention of vanillin bioactivity upon esterification. These findings underscore the potential of vanillin-esterified TEMPO-oxidised nanocellulose as a sustainable, bioactive material for antibacterial applications.

Keywords: Nanocellulose; Esterification; Tempo-Oxidation; Antibacterial

* Corresponding author: Shubhangi P. Patil

Graphical abstract

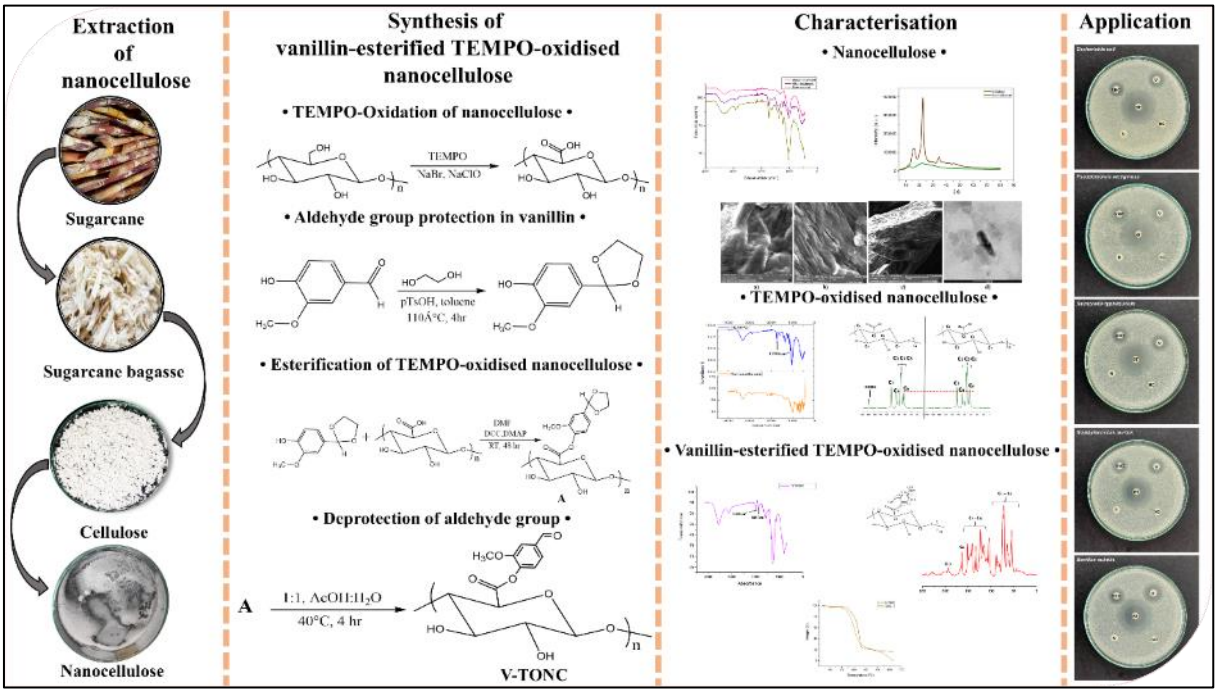

1. Introduction

Nanocellulose, a renewable and biodegradable nanomaterial derived from lignocellulosic biomass, has emerged as a promising alternative to petroleum-based polymers owing to its outstanding mechanical strength, high specific surface area, and rich surface chemistry [1]. Growing environmental concerns related to plastic waste accumulation and the depletion of fossil resources have accelerated research into sustainable nanomaterials, positioning cellulose nanomaterials as key building blocks for advanced functional materials, biocomposites, and biomedical applications [2]. Among various cellulose sources, agricultural residues such as sugarcane bagasse are particularly attractive feedstocks for nanocellulose production. Sugarcane bagasse contains a high cellulose content (approximately 40–50%), is abundantly available as a by-product of the sugar industry, and does not compete with food resources [3]. Valorisation of this agro-industrial waste not only mitigates environmental disposal issues but also generates value-added materials, aligning with the principles of circular bioeconomy and sustainable resource utilisation. Surface chemical modification of nanocellulose is a crucial strategy for tailoring its physicochemical properties and expanding its functional scope. Native nanocellulose contains abundant surface hydroxyl (–OH) groups that serve as reactive sites for chemical functionalization. Various modification approaches, including oxidation, esterification, amidation, carboxymethylation, silylation, sulfonation, epoxidation, and click-chemistry-based conjugation, have been extensively explored to alter surface charge, hydrophobicity, dispersibility, thermal stability, and biological activity [4–7]. Among these, TEMPO-mediated oxidation is particularly attractive due to its high regioselectivity, enabling the conversion of primary hydroxyl groups into carboxylic acid (–COOH) functionalities while preserving the crystalline structure of cellulose. The resulting carboxylated nanocellulose provides versatile reactive sites for subsequent covalent coupling of bioactive molecules through esterification [8].

Sequential modification of nanocellulose via TEMPO oxidation followed by esterification has been widely reported as an effective route to engineer multifunctional biomaterials. Previous studies have demonstrated successful immobilisation of diverse biomolecules on TEMPO-oxidised nanocellulose, resulting in enhanced antimicrobial, antioxidant, and controlled-release properties [9]. For instance, carbodiimide-mediated coupling on TEMPO-oxidised nano fibrillated cellulose has enabled efficient covalent attachment of functional molecules, while esterification with natural resin acids and phenolic compounds has imparted significant antibacterial activity against both Gram-positive and Gram-negative bacteria [10]. These findings highlight the potential of TEMPO-oxidised nanocellulose as a robust platform for the development of bioactive materials.

In this context, vanillin was selected as a bioactive esterification agent owing to its natural origin, excellent biocompatibility, and well-documented antimicrobial and antioxidant properties. Vanillin exerts antibacterial effects through disruption of bacterial cell membrane integrity, depolarisation of membrane potential, and inhibition of intracellular energy metabolism, leading to reduced Adenosine Triphosphate (ATP) synthesis and cell death [11]. It has demonstrated broad-spectrum antimicrobial activity against both Gram-positive and Gram-negative pathogens, including *Staphylococcus aureus*, *Bacillus subtilis*, *Escherichia coli*, *Pseudomonas aeruginosa*, and *Salmonella* species. However, direct incorporation of vanillin into polymeric matrices often suffers from volatility and limited stability, restricting its long-term antimicrobial performance.

The present study addresses these limitations by covalently conjugating vanillin onto TEMPO-oxidised nanocellulose extracted from sugarcane bagasse through an esterification strategy involving aldehyde protection to preserve vanillin's bioactivity. This approach integrates the mechanical robustness and sustainability of nanocellulose with the antimicrobial efficacy of vanillin, yielding a multifunctional bio-nanomaterial. The antibacterial performance of the synthesised vanillin-esterified TEMPO-oxidised nanocellulose (V-TONC) was systematically evaluated against representative Gram-positive (*S. aureus* NCTC 8325, *B. subtilis* QST 713) and Gram-negative (*E. coli* ATCC 12228, *P. aeruginosa* ATCC 25922, *S. typhi* CT18) bacterial strains using the disc diffusion method [12]. This work demonstrates a sustainable and effective strategy for developing bioactive nanocellulose-based materials with potential applications in antimicrobial wound dressings, active food packaging, and biomedical surface coatings.

2. Materials and methods

2.1. Material

Sodium Bromide (NaBr), 2,2,6,6-Tetramethylpiperidin-1-yl)oxyl (TEMPO), Sodium hypochlorite solution (12% chlorine, NaClO), Sodium hydroxide, hydrogen peroxide, Hydrochloric acid, sulphuric acid, toluene, ethanol, Ethylene glycol, p-toluenesulfonic acid (p-TsOH), N, N-Dimethylformamide (DMF), N, N'-Dicyclohexylcarbodiimide (DCC), 4-Dimethylaminopyridine (DMAP), and acetic acid were purchased from Loba Chemie Pvt. Ltd. (Mumbai, India).

2.2. Method

2.2.1. Extraction of nanocellulose

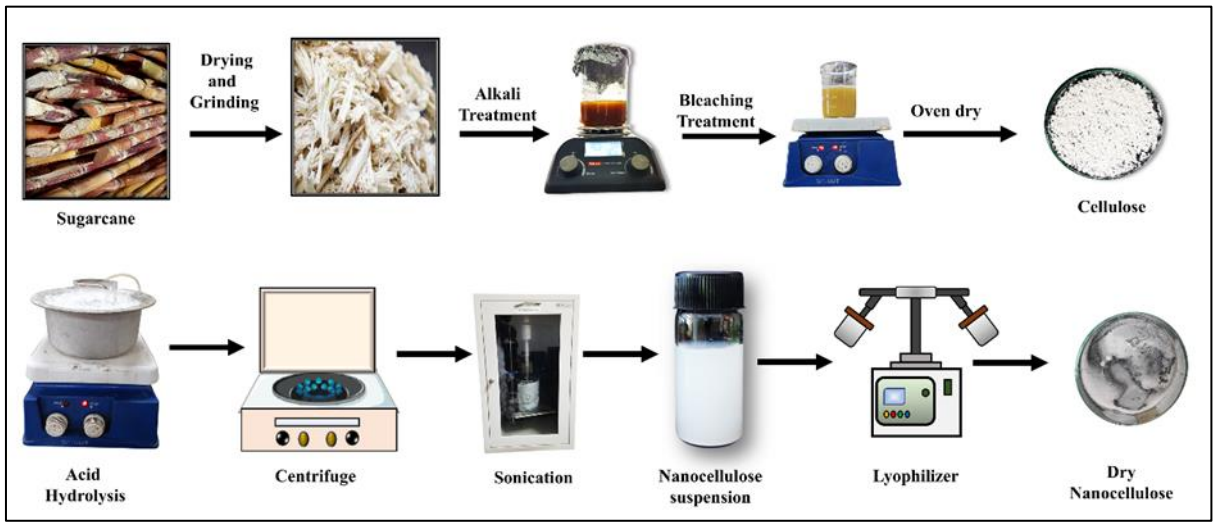

Figure 1 Extraction process of nanocellulose from Sugarcane Bagasse

Sugarcane Bagasse was collected from a farm, thoroughly washed several times with water to remove surface impurities, and then dried. The dried husk was cut into small pieces and ground into a fine powder. Ten grams of this powder were soaked in 100 mL of water for 1 hour and filtered. The residue was washed three times with water to remove any remaining impurities. Subsequently, 100 mL of 4% 1M NaOH solution was added to the residue and stirred at 50 °C for 1 hour. This step, known as alkali treatment, helps remove lignin and hemicellulose. The mixture was then filtered, and the residue was washed thoroughly with water. For bleaching treatment, 100 mL of hydrogen peroxide was added to the residue and stirred at 50 °C for 1 hour to eliminate any remaining impurities(5). The mixture was filtered, washed with water, and dried to obtain a white material, identified as cellulose. Nanocellulose was synthesised

via acid hydrolysis. In this process, 1 g of cellulose was dispersed in 20 mL of water, and 30 mL of chilled 60% H_2SO_4 was added dropwise while maintaining the temperature between 4–5 °C [13]. After the acid addition was complete, the reaction mixture was poured into 200 mL of chilled water and stirred vigorously. The excess acid was removed by repeated washing with distilled water using centrifugation at 10,000 rpm for 10 minutes, repeated four times. The resulting suspension was then subjected to probe sonication for 15 minutes at 80% amplitude with a pulse interval of 10 seconds, maintaining the temperature between 4–5 °C to prevent overheating. The obtained nanocellulose suspension was stored in a refrigerator for further use (Figure 1) [14,15].

2.2.2. TEMPO-Oxidation of nanocellulose

A 10 mL nanocellulose suspension (0.2%) was added to 100 mL of a solution containing TEMPO (0.031 g) and sodium bromide (0.60 g). The mixture was stirred at 500 rpm for 30 min in a round-bottom flask. Subsequently, 2.56 mL of sodium hypochlorite (NaClO) was added dropwise under continuous stirring, and the reaction was allowed to proceed for 3 h. During the addition of NaClO, oxidation commenced, causing a drop in pH. The pH was maintained between 10 and 11 by adding 0.5 M NaOH. The completion of the reaction was indicated by a decrease in NaOH consumption and stabilisation of the pH at approximately 10.5. The reaction was quenched by adding 10 mL of ethanol. The product was then washed thoroughly with distilled water. Protonation of the oxidised nanocellulose was carried out by adding 1 M HCl until the pH reached 1, followed by stirring for 15 min. TEMPO-oxidised nanocellulose (TONC) product was subsequently washed with distilled water until the pH reached 4 and then stored at 4 °C (Scheme 1) [16–18].

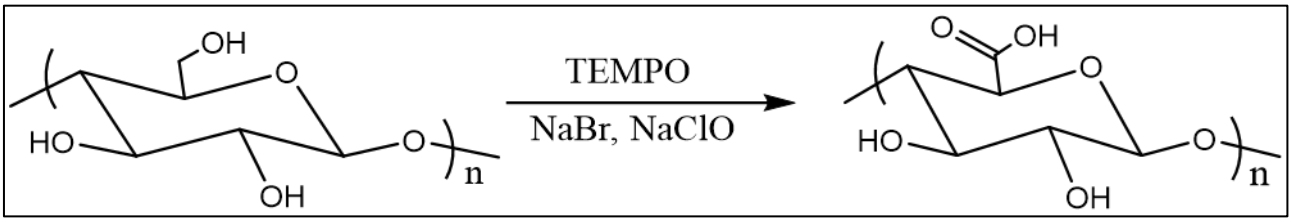

Scheme 1 Schematic representation of TEMPO-Oxidation of nanocellulose

2.2.3. Conductometric titration

The degree of oxidation of oxidised nanocellulose was determined by conductometric titration. 50 mg each of nanocellulose and oxidised nanocellulose were dispersed in 15 mL of 0.01 M HCl solution and stirred for 5 minutes. The titration of these suspensions was done with a 0.01 M NaOH solution under continuous stirring. Conductivity was measured after every 1 mL addition of NaOH. The content of carboxyl groups (degree of oxidation) was determined by the equation number 1(Eq 1) given below,

$$DO = \frac{162 \times c \times (V_2 - V_1)}{w - 36(V_2 - V_1) \times c} \quad \text{.....(Eq. 1)}$$

Where:
V_1 – volume of NaOH (L) at the first point of inflexion of the titration curve,
V_2 – the amount of NaOH (L) at the second point of inflexion of the titration curve,
c – concentration of NaOH [M],
w – weight of the cellulose sample [g].

The titration was repeated three times. Mean results were employed to determine the total acidic group content [17,19].

2.2.4. Esterification of Tempo oxidised nanocellulose

To selectively functionalize TONC with vanillin via esterification of its phenolic hydroxyl group, the aldehyde was first protected as a cyclic acetal using ethylene glycol and p-TsOH catalysis in refluxing toluene with a Dean-Stark trap at 110°C for 4hr, yielding the 1,3-dioxolane derivative in 92% isolated yield after recrystallisation (Scheme 2)[20,21], The protected vanillin (2 equiv relative to TONC-COOH, ~1.2 mmol/g) was then coupled to a 1 wt% TONC suspension in DMF using DCC (2 equiv) and DMAP (0.2 equiv) at room temperature for 48 h, forming the ester linkage while the acetal remained intact under neutral conditions; filtration of dicyclohexylurea and freeze-drying afforded the intermediate in 82% yield. Mild acid hydrolysis (1:1 AcOH: H_2O, 40°C, 4 h) selectively deprotected the acetal to regenerate the aldehyde, followed by neutralisation, centrifugation, and lyophilisation to give vanillin-esterified TONC (V-TONC) (Scheme 3).[22,23].

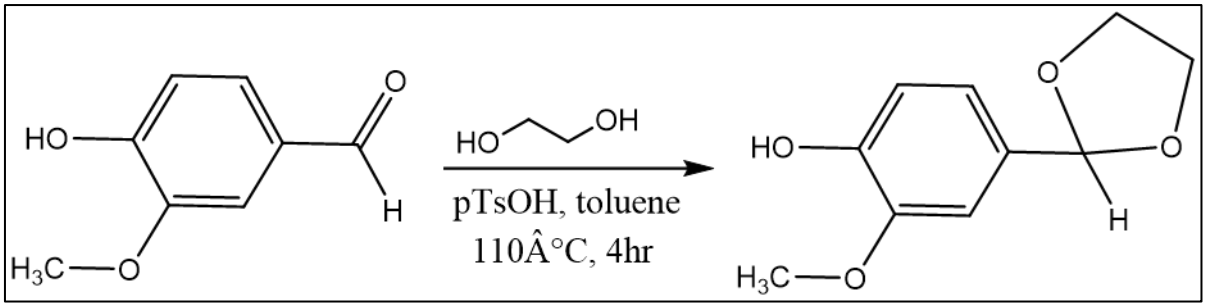

Scheme 2 Schematic representation of aldehyde group protection in vanillin.

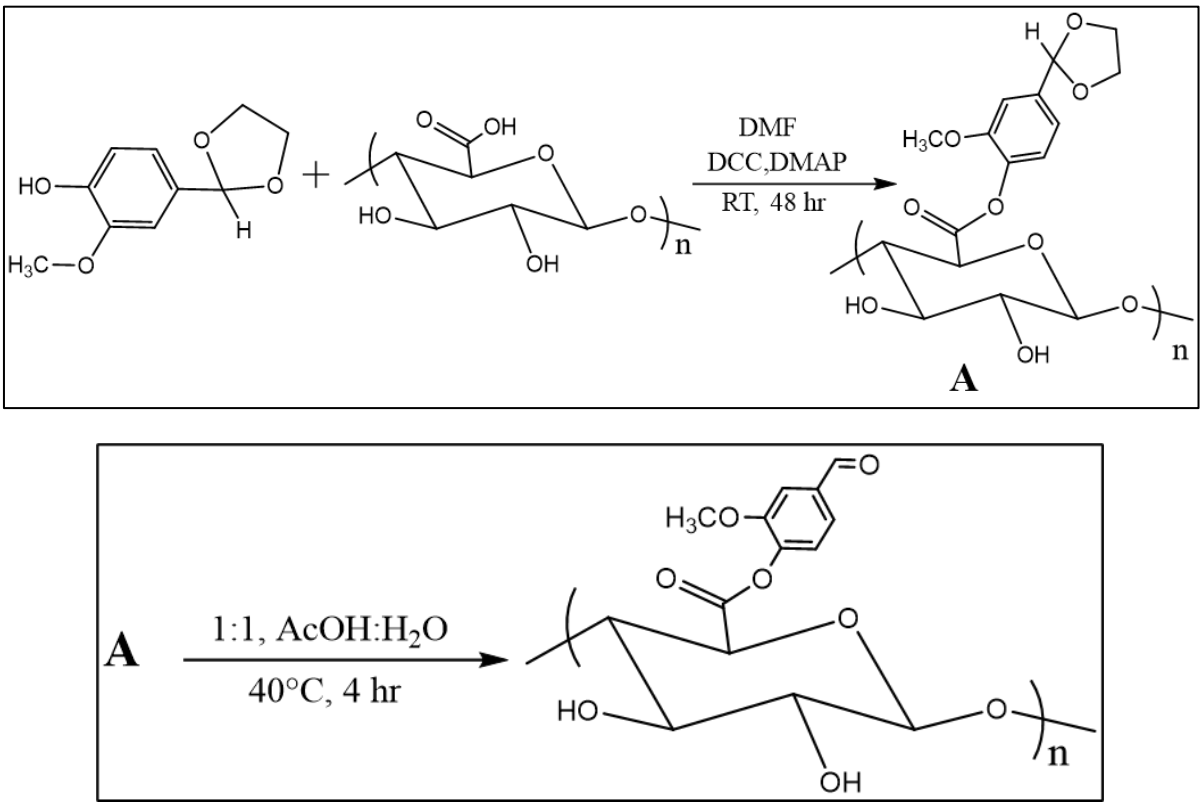

Scheme 3 Esterification of TEMPO-oxidised nanocellulose (TONC) with aldehyde-protected vanillin and deprotection of the aldehyde group

2.2.5. Antibacterial activity of ferulic acid modified nanocellulose

To evaluate the antibacterial activity of vanillin-esterified TONC and nanocellulose, Gram-positive bacteria (*Staphylococcus aureus* NCTC8325, *Bacillus subtilis* QST713) and Gram-negative bacteria (*Escherichia coli* ATCC12228, *Pseudomonas aeruginosa* ATCC25922, *Salmonella typhi* CT18) were used for the disc diffusion method [12,24]. Bacteria were distributed evenly onto the nutrient medium in sterile petri plates. Each nutrient agar plate contained four sterile discs (7mm Diameter) that were loaded (20µL) with Vanillin (V), vanillin-esterified TEMPO-oxidised nanocellulose (VNC), nanocellulose (NC), and a negative control (sterile distilled water) (N). For positive control (PC), Chloramphenicol was used. The antibacterial activity of the nanocellulose was assessed by measuring the zone of inhibition after 24-hour incubation at 37°C [25–28].

2.3. Characterisation

2.3.1. Structural Analysis

The morphological features and surface topology of the nanocellulose samples were examined using field emission scanning electron microscopy (FE-SEM) on a QUANTA 200 instrument, operating at an accelerating voltage of 30 kV. High-resolution transmission electron microscopy (HRTEM) images were acquired using a JEOL model 1200 Ex II microscope (JEOL, Tokyo, Japan) at 80 kV accelerating voltage with 200-fold magnification to visualise the nanostructural details of the prepared materials.

2.3.2. Chemical Composition and Functional Group Identification

Fourier-transform infrared spectroscopy (FTIR) was employed to investigate the surface chemical composition and functional groups present in the modified nanocellulose samples. Measurements were conducted across the spectral range of 4000–500 cm^{-1} to capture the complete infrared absorption profile characteristic of the material.

2.3.3. Thermal Behaviour Assessment

The thermal stability profile of the nanocellulose materials was determined through thermogravimetric analysis (TGA) combined with differential thermal analysis (DTA) using a TGA55 instrument (TA Instruments, USA). Samples were heated from 20 °C to 900 °C at a linear heating rate of 20 °C/min under controlled atmospheric conditions to evaluate decomposition pathways and thermal transition temperatures.

2.3.4. Solid-State Nuclear Magnetic Resonance Spectroscopy (^{13}C SS-NMR)

Carbon-13 solid-state nuclear magnetic resonance (^{13}C SS-NMR) spectroscopy was performed on a Bruker Avance II-300 spectrometer to characterise the carbon environments and structural variations between native nanocellulose and chemically modified nanocellulose samples. This technique provided insights into the molecular structure and the effectiveness of the chemical modifications.

2.3.5. Crystalline Structure Evaluation

X-ray diffraction (XRD) analysis was carried out using a RIGAKU MINI FLEX-600 diffractometer to characterise the crystalline architecture of the nanocellulose samples. The measurement parameters included a diffraction angle range (2θ) of 10° to 70°, with a scanning speed of 5° per minute. The crystallinity index (CI) of each sample was calculated using the empirical method developed by Segal, as described in Equation 2.

$$\boldsymbol{CI}(\%) = \frac{\boldsymbol{I_{200}}}{\boldsymbol{I_{200}-I_{am}}} \times \mathbf{100} \ldots\ldots\ldots\ldots\ldots\ldots\ldots\ldots\ldots\ldots\textbf{Eq. 2}$$

Here, I_{200} represents the maximum intensity of the principal (200) crystal plane, while I_{am} corresponds to the diffraction intensity associated with the amorphous region of cellulose [29].

3. Result and Discussion

3.1. Nanocellulose

The Fourier Transform Infrared (FTIR) spectroscopy demonstrates progressive removal of non-cellulosic components through sequential chemical treatments of sugarcane bagasse, as shown in Figure 2. The raw material exhibits characteristic peaks for cellulose, hemicellulose, and lignin, including broad O-H stretching at 3000-3500 cm^{-1}, aromatic C=C stretching at 1600-1500 cm^{-1} (lignin), carbonyl C=O at 1735 cm^{-1} (hemicellulose), and glycosidic C-O-C stretching at 1165 and 1034 cm^{-1}. [30,31]

Following alkali treatment, the aromatic peaks at 1600-1500 cm^{-1} significantly diminish due to lignin removal, while the carbonyl peak at 1735 cm^{-1} decreases as hemicellulose is extracted. The cellulose-specific peaks at 1165 cm^{-1}, 1034 cm^{-1}, and 890 cm^{-1} (β-glycosidic C1-H deformation) become more pronounced and sharper. After bleaching treatment, complete elimination of aromatic lignin peaks and carbonyl peaks confirms pure cellulose isolation, with characteristic cellulose bands at 1370-1430 cm^{-1} (C-H bending), 1047-1061 cm^{-1} (pyranose ring C-O stretching), and 890 cm^{-1} showing maximum intensity and crystalline definition. The spectroscopic progression clearly validates the successful extraction of pure cellulose through the systematic removal of lignin and hemicellulose via sequential chemical treatments [32].

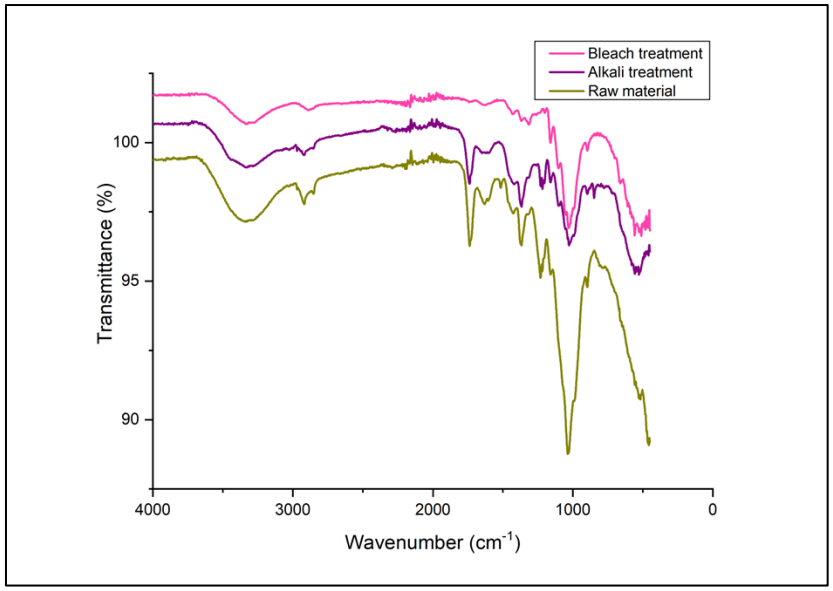

Figure 2 FTIR spectra of cellulose extracted from sugarcane bagasse showing raw material (olive), alkali treatment (purple), and bleached cellulose (pink).

Figure 3 displays the XRD patterns for both cellulose and nanocellulose. Each sample shows distinct diffraction peaks that are indicative of the crystalline structure of cellulose. The peaks at around 2θ = 15.0°, 16.5°, and 22.5° confirm the presence of cellulose [32,33]. Notably, the nanocellulose sample demonstrates a marked increase in peak intensity, especially at 2θ = 22.5°, which aligns with the characteristic crystalline plane of cellulose. This suggests a significant enhancement in the crystallinity index, rising from 45% in cellulose to 88% in nanocellulose. This improvement is likely due to the removal of amorphous substances like hemicellulose and lignin during chemical treatments, which reveal and enhance the crystalline regions of cellulose. Furthermore, the mechanical breakdown involved in preparing nanocellulose probably results in a more orderly arrangement of cellulose chains, leading to sharper and more pronounced peaks. The broader and less intense peaks in the cellulose sample indicate a greater presence of amorphous areas, which is common in biomass-derived cellulose before it undergoes purification and size reduction. Conversely, the sharper peaks in the nanocellulose spectrum suggest a more defined and crystalline structure, advantageous for applications that require high mechanical strength and thermal stability. These findings confirm that nanocellulose maintains the crystalline properties of cellulose [34].

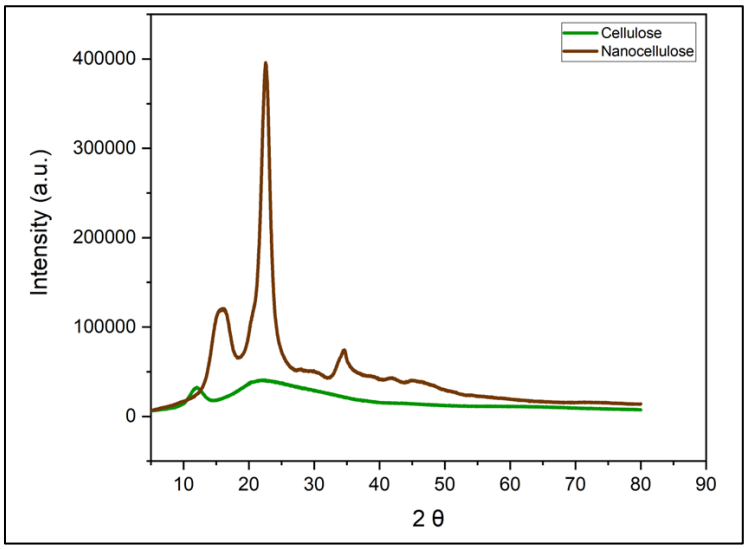

Figure 3 X-ray diffraction (XRD) patterns of cellulose and nanocellulose.

As shown in Figure 4, Scanning electron microscopy (SEM) of the raw sugarcane bagasse reveals a compact, heterogeneous surface with tightly bound fibrillar structures, indicating the presence of lignin, hemicellulose and other

non-cellulosic components that shield the underlying cellulose microfibrils [35]. Following alkali treatment, the fibres exhibit a more open, layered morphology with partially separated fibrils and increased surface roughness, reflecting effective removal of hemicellulose and partial delignification, which facilitates fibrillation and improves accessibility of the cellulose network. Subsequent bleaching produces a cleaner, more fibrillated structure with distinct, loosely packed cellulose bundles and reduced surface impurities, confirming substantial elimination of residual lignin and chromophoric components and yielding purified cellulose suitable for nanocellulose production. Transmission electron microscopy (TEM) of the obtained nanocellulose shows individualised, high-aspect-ratio cellulose nanofibers with an average width of approximately 35 nm and length of about 270 nm, demonstrating successful nanoscale disintegration of the bleached cellulose and confirming the formation of nanocellulose [14].

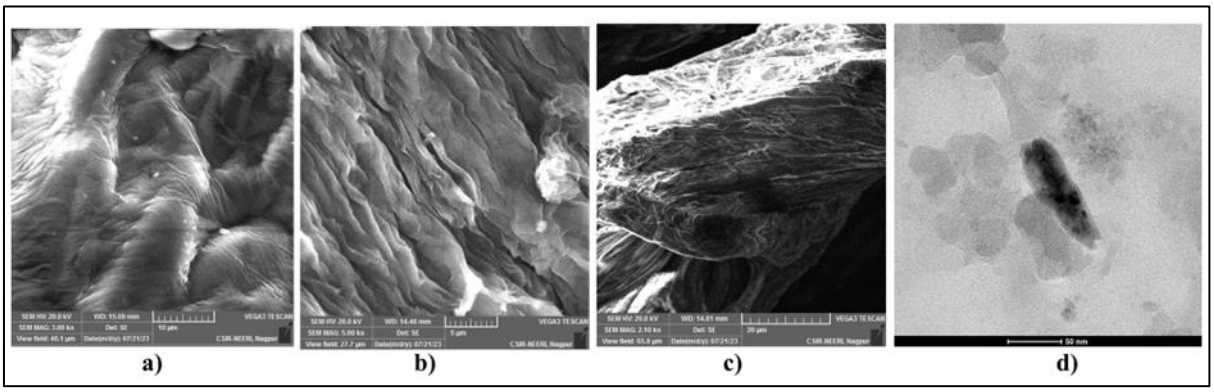

Figure 4 Morphological transformation of sugarcane bagasse during nanocellulose isolation: SEM image of a) raw sugarcane bagasse; b) alkali-treated fibres; c) bleached cellulose, (d) TEM image of the resulting nanocellulose.

3.2. TEMPO-Oxidised nanocellulose

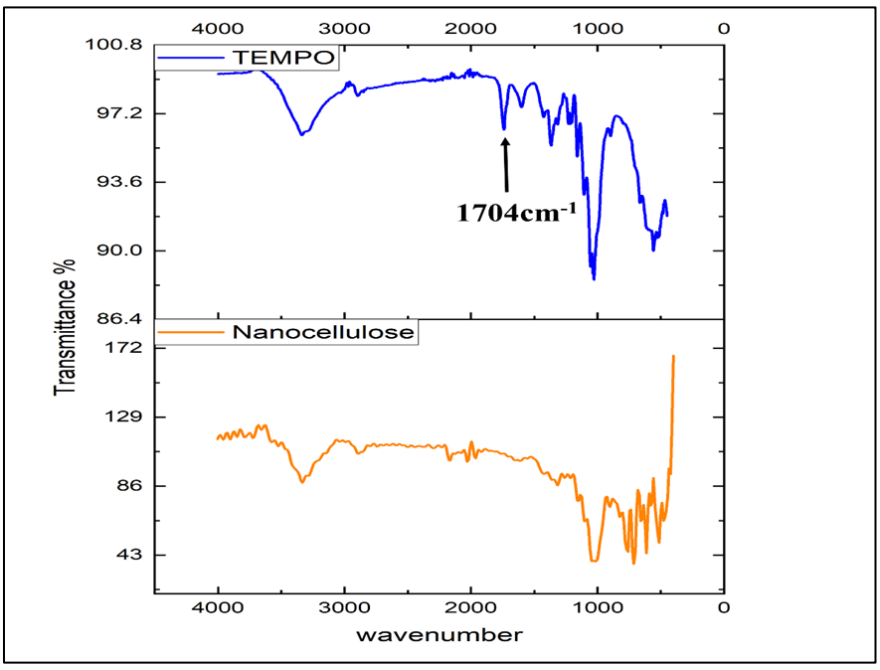

Figure 5 IR graph of NC and TONC.

Fourier transform infrared (FTIR) spectroscopy was employed to characterise the chemical composition and functional group changes in nanocellulose before and after TEMPO oxidation shown in Figure 5. The FTIR spectrum of pristine nanocellulose displays the characteristic absorption bands of cellulose, including a broad O–H stretching band around 3300–3400 cm^{-1}, C–H stretching vibrations near 2900–3000 cm^{-1}, and dominant C–O stretching bands in the 1000–1200 cm^{-1} region, with minimal absorbance in the carbonyl region, confirming the absence of significant oxidized functional groups in the unmodified material. Following TEMPO oxidation, the spectrum of TEMPO-oxidised nanocellulose reveals a distinctive new absorption band at 1704 cm^{-1}, which is characteristic of C=O stretching in

carboxylic acid groups (–COOH), indicating successful selective oxidation of the C6 primary hydroxyl groups on the cellulose backbone. The emergence of this strong carbonyl band at 1704 cm^{-1} in the TEMPO-oxidised sample, combined with the preservation of the cellulose skeletal vibrations and O–H stretching regions, demonstrates that the TEMPO oxidation process effectively introduces anionic carboxyl functionality to the nanocellulose surface without significant structural degradation of the polysaccharide backbone [8,18,19].

As shown in Figure 6, the structural validation of cellulose nanofibrils modified through TEMPO-mediated oxidation was achieved using solid-state ^{13}C NMR spectroscopy. The spectra for both NC and TONC exhibit the characteristic signal clusters of the cellulose: the anomeric carbon (C_1) resonance at 100–110 ppm, the C_4 crystalline and amorphous doublet at 80–95 ppm, and the overlapping resonances for the pyranose ring carbons C_2, C_3, and C_5 in the 70–80 ppm range. The successful introduction of carboxylate functionalities is clearly indicated by the appearance of a new resonance at approximately 175 ppm, corresponding to the carbonyl carbon of the C_6 carboxylate groups (36). Notably, the resonance for the primary hydroxyl-bearing C_6 carbon at 60–70 ppm remains visible in the oxidised spectrum, though with a significant reduction in integral intensity compared to the non-oxidised control. This finding confirms that the oxidation process did not completely convert all primary hydroxyl groups; instead, a specific fraction, mainly those on the solvent-accessible fibril surfaces, was selectively transformed into carboxylic acid moieties, while the C_6 hydroxyls within the crystalline core remained chemically unaltered.

The degree of oxidation (DO) of the TEMPO-oxidised nanocellulose was evaluated using conductometric titration. The conductometric titration data were analysed according to Equation (1) to quantify the carboxylate content introduced during the oxidation process. Based on this analysis, the degree of oxidation was calculated to be 0.08, indicating successful conversion of primary hydroxyl groups on the nanocellulose surface into carboxyl groups.

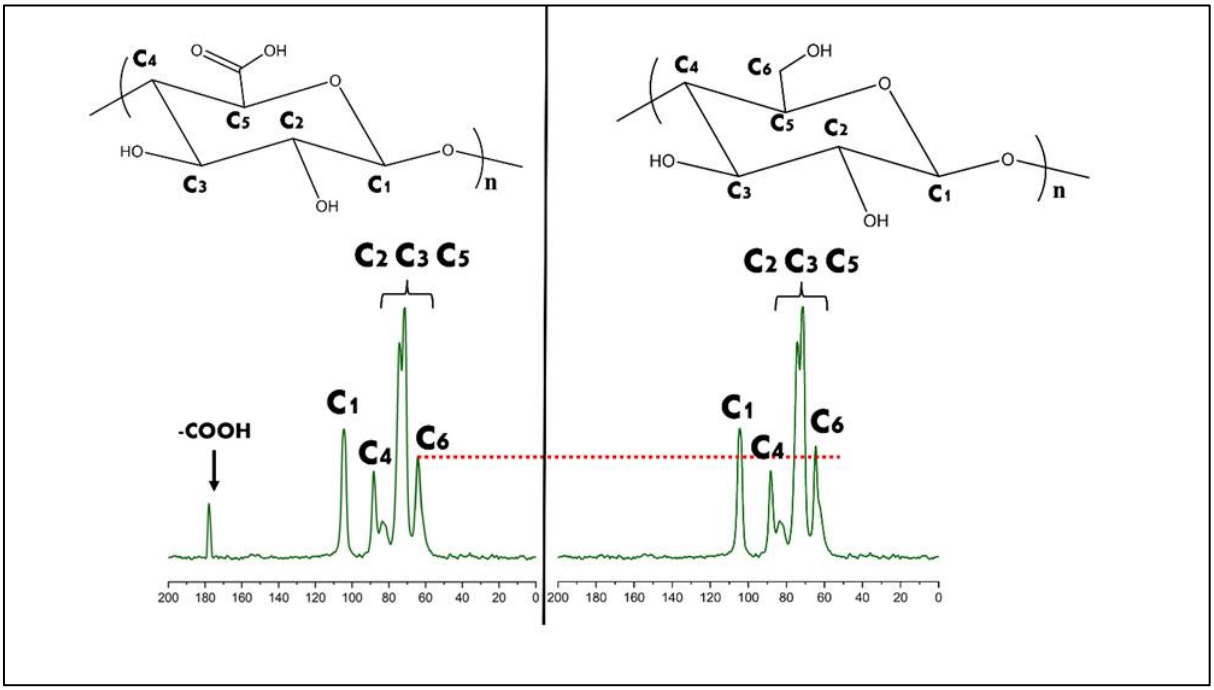

Figure 6 ^{13}C SS-NMR of TONC and NC.

3.3. Esterified oxidised nanocellulose

The Fourier transform infrared (FTIR) spectrum of vanillin-esterified TEMPO-oxidised nanocellulose (V-TONC) provides comprehensive evidence of successful chemical modification, characterised by distinct spectral features arising from both the nanocellulose backbone and the introduced vanillin moieties (Figure 7). A broad absorption band centred around 3300–3400 cm^{-1} is observed, corresponding to the O–H stretching vibrations of residual hydroxyl groups involved in intra- and intermolecular hydrogen bonding. The peak at approximately 2900 cm^{-1} is attributed to the C–H stretching vibrations of the cellulose backbone (–CH and $–CH_2$ groups) [37].

Crucially, the spectrum confirms esterification through significant changes in the carbonyl region. The characteristic peak at 1704 cm^{-1}, typically associated with the –C=O stretching of free carboxylic acid groups in TEMPO-oxidised

nanocellulose (TONC), is absent. Instead, a new, sharp peak appears at 1750 cm^{-1}, which is assigned to the –C=O stretching vibration of the newly formed ester linkages. Concurrently, a distinct peak emerges at 1687 cm^{-1}, corresponding to the C=O stretching of the aromatic aldehyde group inherent to the vanillin substituent. Further evidence of vanillin incorporation is provided by the appearance of aromatic skeletal vibrations. Peaks in the range of 1500–1600 cm^{-1} (specifically around 1515 cm^{-1} and 1590–1600 cm^{-1}) are characteristic of the C=C stretching vibrations of the benzene ring in the vanillin structure. Additionally, the intense bands in the 1000–1100 cm^{-1} region are dominated by the C–O–C pyranose ring skeletal vibrations of the cellulose backbone, but likely overlap with the C–O stretching vibrations of the aromatic ether (–OCH_3) and phenolic ester groups introduced by vanillin. The collective presence of these bands, specifically the ester carbonyl at 1750 cm^{-1}, the aldehyde carbonyl at 1687 cm^{-1}, and the aromatic ring vibrations alongside the disappearance of the carboxylic acid peak, conclusively demonstrates the successful covalent attachment of vanillin to the TONC surface via ester bonds [38].

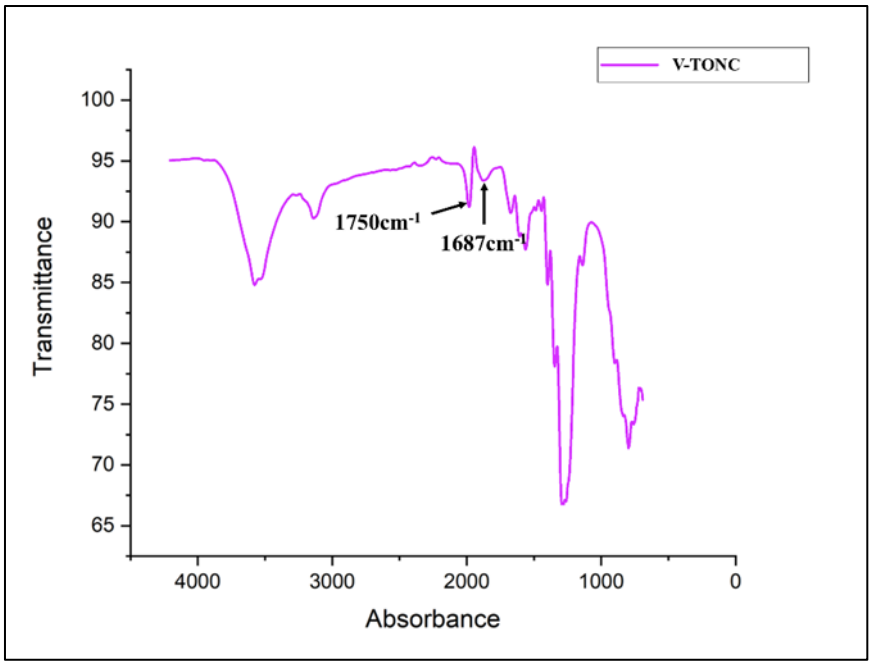

Figure 7 IR graph of vanillin-esterified TEMPO-oxidised nanocellulose

In Figure 8, the solid-state ^{13}C NMR spectrum of vanillin-esterified TEMPO-oxidised nanocellulose (V-TONC) provides conclusive structural evidence for the successful covalent attachment of vanillin to the nanocellulose surface. The spectrum anomeric carbon (C_1) resonance at 100–110 ppm, the C_4 crystalline and amorphous doublet at 80–95 ppm, and the overlapping resonances for the pyranose ring carbons C_2, C_3, and C_5 in the 70–80 ppm range. A critical diagnostic feature is the chemical shift of the carbonyl carbon at the C_6 position; in the precursor TEMPO-oxidised nanocellulose (TONC), the C_6-carboxylate carbon typically resonates at approximately 175 ppm. In the V-TONC spectrum, this peak undergoes a significant upfield shift to 169 ppm, which is indicative of the formation of an ester linkage between the C_6-carboxyl group of nanocellulose and the phenolic hydroxyl group of vanillin. Furthermore, the introduction of vanillin moieties is substantiated by the appearance of distinct aromatic carbon signals in the 110–155 ppm region (labelled C_7–C_{12}), corresponding to the vanillin benzene ring carbons. Specifically, the peak at 191 ppm is assigned to the aldehydic carbonyl carbon (C_{13}) of the vanillin pendant group, confirming that the aldehyde functionality remains intact after esterification. Collectively, the shift of the C_6 resonance to 169 ppm, the presence of aromatic signals, and the retention of the aldehyde peak at 191 ppm provide strong spectroscopic proof of the successful synthesis of V-TONC [39,40].

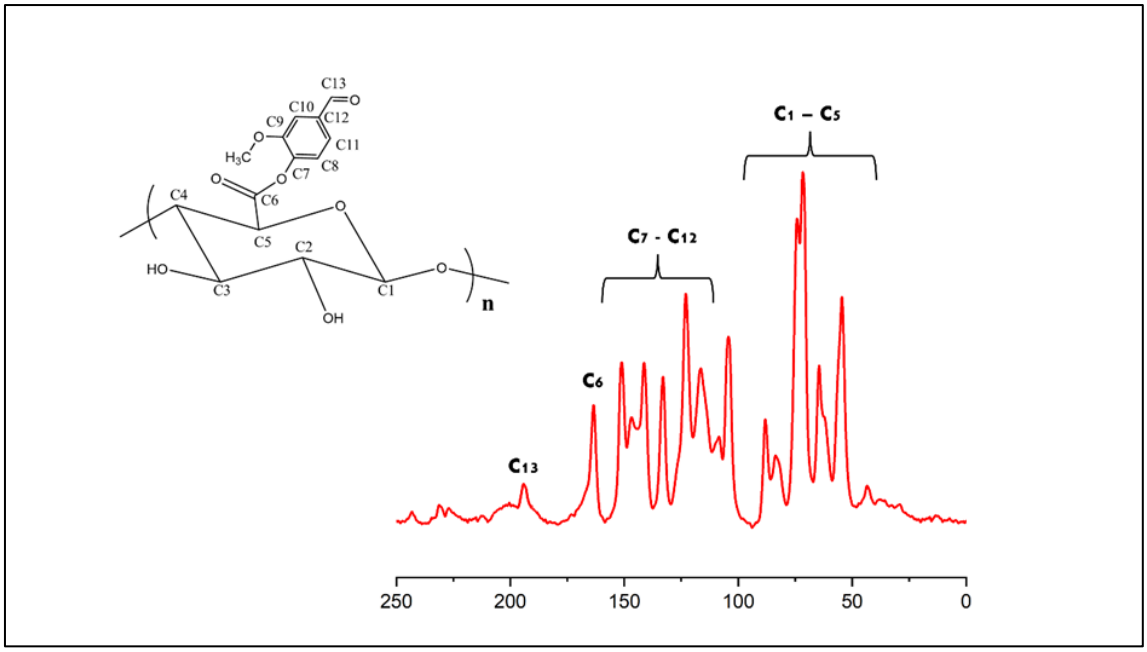

Figure 8 ^{13}C SS-NMR of V-TONC

The thermal stability of TEMPO-oxidised nanocellulose (TONC) and vanillin-esterified TEMPO-oxidised nanocellulose (V-TONC) was evaluated using thermogravimetric analysis (TGA), as shown in Figure 9. Both samples exhibited a similar initial weight loss of approximately 3–4% below 120 °C, corresponding to the evaporation of physically adsorbed moisture. However, the functionalization with vanillin significantly altered the main thermal decomposition profile. The onset degradation temperature decreased by approximately 30 °C, shifting from 245 °C for TONC to 215 °C for V-TONC. Similarly, the temperature at 50% weight loss dropped from 345 °C in TONC to 310 °C in the esterified sample. This reduction in thermal stability can be attributed to the introduction of bulky aromatic vanillin groups, which likely disrupt the compact intermolecular hydrogen bonding network and crystalline order of the nanocellulose fibrils, coupled with the relative thermal lability of the newly formed ester linkages. Furthermore, the residual mass at 600 °C revealed a distinct difference in carbonisation behaviour; while TONC retained a significant char yield of 16.5%.

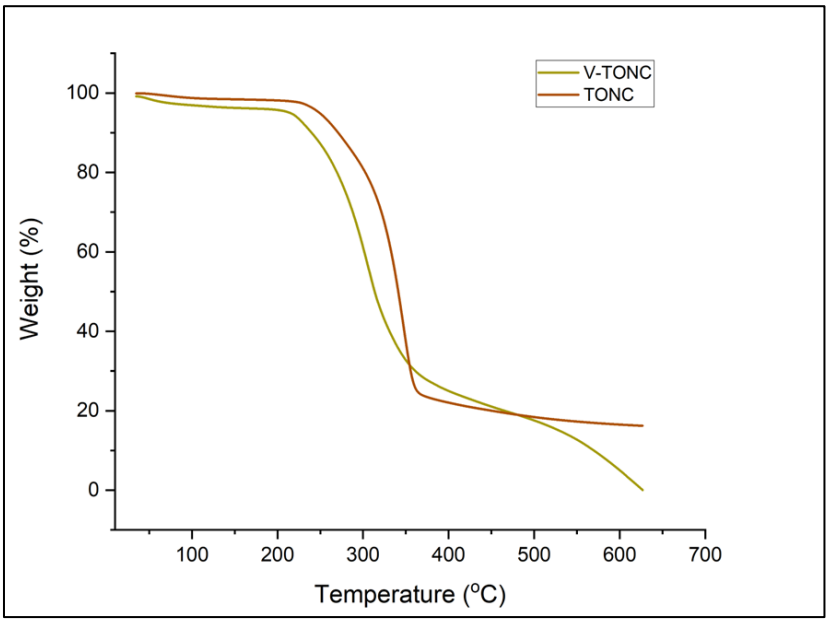

Figure 9 TGA graph of TONC and V-TONC

The antibacterial disc diffusion results, as depicted in Figure 10 and Table 1, demonstrate that nanocellulose exhibits enhanced antibacterial activity following esterification with vanillin, resulting in the development of an active antibacterial material. Vanillin (V) alone exhibited significant antibacterial effects against all tested strains, with inhibition zones ranging from 23.66 mm to 25.33 mm. Notably, vanillin-esterified TEMPO-oxidised nanocellulose also exhibited substantial zones of inhibition (20.33–21.66 mm), confirming that the modified Vanillin retained its bioactivity and imparted functional properties to the nanocellulose matrix. In contrast, unmodified nanocellulose (NC) and the negative control (N) demonstrated no inhibitory effects, verifying that the antibacterial property arises specifically from chemical modification. The positive control (PC), Chloramphenicol, consistently showed large inhibition zones (34.66–35.00 mm), serving as a reference. These findings suggest that vanillin-esterified TEMPO-oxidised nanocellulose can function as a bioactive antibacterial material suitable for applications in wound dressings, food packaging, and biomedical coatings.

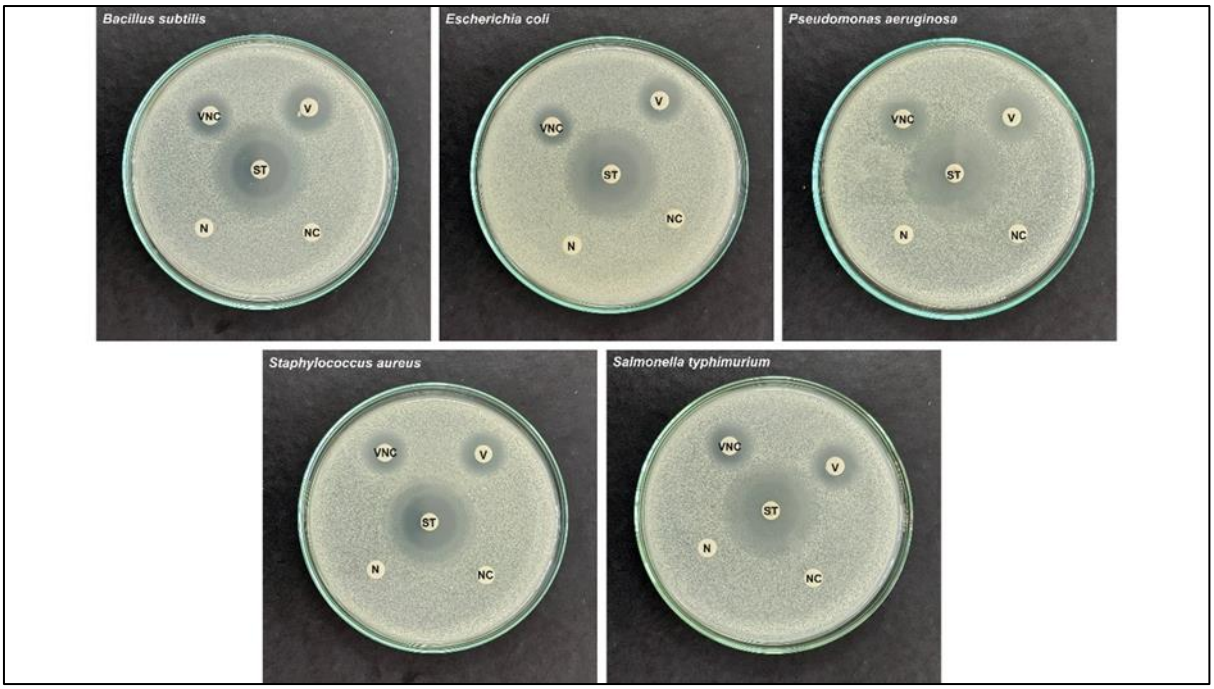

Figure 10 Antibacterial activity of nanocellulose (NC), Vanillin (V), and vanillin-esterified TEMPO-oxidised nanocellulose (VNC) against *Bacillus subtilis, Escherichia coli, Pseudomonas aeruginosa, Staphylococcus aureus,* and *Salmonella typhi*.

Table 1 Inhibition zones of all bacteria

SN	Bacterial strain	V	VNC	N	NC	ST
1	*Bacillus subtilis* QST713	23.66 ± 0.57	20.33 ± 0.57	0	0	34.66 ± 0.57
2	*Escherichia coli* ATCC12228	25.00 ± 1.00	21.33 ± 0.57	0	0	34.66 ± 0.57
3	*Staphylococcus aureus* NCTC8325	24.66 ± 1.15	21.33 ± 0.57	0	0	35.00 ± 0.00
4	*Salmonella typhi* CT18	25.33 ± 0.57	21.66 ± 1.15	0	0	34.66 ± 0.57
5	*P. aeruginosa* ATCC25922	25.33 ± 0.57	21.66 ± 1.15	0	0	35.00 ± 0.00

4. Conclusion

The study successfully demonstrated the extraction of nanocellulose from sugarcane bagasse, followed by its selective surface modification through TEMPO-mediated oxidation and subsequent esterification with vanillin. Comprehensive characterisation confirmed the effective removal of non-cellulosic components, enhanced crystallinity, and the introduction of carboxyl and ester functionalities without compromising the cellulose backbone. The covalent attachment of vanillin was verified by distinct spectroscopic signatures, including FTIR peak 1750 cm^{-1} and solid-state ^{13}C NMR, peak at 169 ppm of ester bond, while thermal analysis revealed a decrease in thermal stability due to ester linkage formation and disruption of hydrogen bonding. Importantly, the vanillin-esterified TEMPO-oxidised nanocellulose exhibited significant antibacterial activity against both Gram-positive and Gram-negative bacteria, comparable to pure vanillin, indicating retention of bioactivity. These findings establish vanillin-functionalized nanocellulose as a promising sustainable bioactive material with potential applications in wound dressings, food packaging, and biomedical coatings.

Compliance with ethical standards

Acknowledgments

We acknowledge and are grateful to the Director of the Institute of Science, Mumbai, for the support and recognition. No financial support was received for the authorship or publication of this article.

Disclosure of conflict of interest

The authors declare that they have no known competing financial interests or personal relationships that could have appeared to influence the work reported in this paper. No conflict of interest exists.

References

[1] Lu Y, Tekinalp HL, Eberle CC, Peter W, Kumar Naskar A, Ozcan S. Nanocellulose in polymer composites and biomedical applications. TAPPI J. 2014 July 1;13(6):47–54.

[2] Lamm ME, Li K, Qian J, Wang L, Lavoine N, Newman R, et al. Recent Advances in Functional Materials through Cellulose Nanofiber Templating. Adv Mater. 2021 Mar;33(12):2005538.

[3] Pula B, Ramesh S, Pamidipati S, Doddipatla P. A comparative study of greener alternatives for nanocellulose production from sugarcane bagasse. Bioresour Bioprocess. 2021 Dec;8(1):132.

[4] Bangar SP, Harussani MM, Ilyas RA, Ashogbon AO, Singh A, Trif M, et al. Surface modifications of cellulose nanocrystals: Processes, properties, and applications. Food Hydrocoll. 2022 Sept;130:107689.

[5] Mavlankar GR, Bhatu MN, Baikar PP, Patil SP. Unlocking the Potential of Nanocellulose: Transforming Cellulose Into a Sustainable Resource for Innovative Applications. ChemistrySelect. 2024 Nov;9(44):e202402065.

[6] Geng S, Yao K, Zhou Q, Oksman K. High-Strength, High-Toughness Aligned Polymer-Based Nanocomposite Reinforced with Ultralow Weight Fraction of Functionalized Nanocellulose. Biomacromolecules. 2018 Oct 8;19(10):4075–83.

[7] Ghasemlou M. Surface modifications of nanocellulose: From synthesis to high-performance nanocomposites. Prog Polym Sci. 2021;52.

[8] Isogai A, Zhou Y. Diverse nanocelluloses prepared from TEMPO-oxidized wood cellulose fibers: Nanonetworks, nanofibers, and nanocrystals. Curr Opin Solid State Mater Sci. 2019 Apr;23(2):101–6.

[9] Kupnik K, Primožič M, Kokol V, Leitgeb M. Nanocellulose in Drug Delivery and Antimicrobially Active Materials. Polymers. 2020 Nov 27;12(12):2825.

[10] Abouhmad A, Dishisha T, Amin MA, Hatti-Kaul R. Immobilization to Positively Charged Cellulose Nanocrystals Enhances the Antibacterial Activity and Stability of Hen Egg White and T4 Lysozyme. Biomacromolecules. 2017 May 8;18(5):1600–8.

[11] Kamat JP, Ghosh A, Devasagayam TPA. Vanillin as an antioxidant in rat liver mitochondria: Inhibition of protein oxidation and lipid peroxidation induced by photosensitization. Mol Cell Biochem. 2000 June;209(1–2):47–53.

[12] Baikar PP, Mavlankar GR, Chavan AK, Rangadal DN, Bhatu MN, Tirmali P, et al. Synthesis of Ag@ZnO/Cellulose Nanocomposites using *Blumea Lacera* Plant for Antibacterial Activity and Removal Of Methylene Blue. ChemistrySelect. 2025 Oct;10(39):e04404.

[13] Baikar PP, Mavlankar GR, Chavan AK, Rangadal DN, Bhatu MN, Tirmali P, et al. Synthesis of Ag@ZnO/Cellulose Nanocomposites using *Blumea Lacera* Plant for Antibacterial Activity and Removal Of Methylene Blue. ChemistrySelect. 2025 Oct;10(39):e04404.

[14] Wulandari WT, Rochliadi A, Arcana IM. Nanocellulose prepared by acid hydrolysis of isolated cellulose from sugarcane bagasse. IOP Conf Ser Mater Sci Eng. 2016 Feb 5;107:012045.

[15] Patil S, Mavlankar GR, Tayade RR. NANOCELLULOSE FROM SUGARCANE BAGASSE: SYNTHESIS AND CHARACTERIZATION. nternational Journal of Current Research. 2023 Oct;15(10):26193–6.

[16] Habibi Y, Chanzy H, Vignon MR. TEMPO-mediated surface oxidation of cellulose whiskers. Cellulose. 2006 Dec;13(6):679–87.

[17] Pawcenis D, Twardowska E, Leśniak M, Jędrzejczyk RJ, Sitarz M, Profic-Paczkowska J. TEMPO-oxidized cellulose for in situ synthesis of Pt nanoparticles. Study of catalytic and antimicrobial properties. Int J Biol Macromol. 2022 July;213:738–50.

[18] Lal SS, Mhaske ST. TEMPO-oxidized cellulose nanofiber/kafirin protein thin film crosslinked by Maillard reaction. Cellulose. 2019 July;26(10):6099–118.

[19] Habibi Y, Chanzy H, Vignon MR. TEMPO-mediated surface oxidation of cellulose whiskers. Cellulose. 2006 Dec;13(6):679–87.

[20] Khan A, Salim S, Masaud SM, Ahmad A, Akhtar MF, Mandukhail SR. Antiurolithic activity of vanillin in ethylene glycol-induced hyperoxaluric rat model. Urolithiasis. 2025 Mar 21;53(1):54.

[21] Zhang H, Yong X, Zhou J, Deng J, Wu Y. Biomass Vanillin-Derived Polymeric Microspheres Containing Functional Aldehyde Groups: Preparation, Characterization, and Application as Adsorbent. ACS Appl Mater Interfaces. 2016 Feb 3;8(4):2753–63.

[22] Li T, Rosazza JPN. Biocatalytic Synthesis of Vanillin. Appl Environ Microbiol. 2000 Feb;66(2):684–7.

[23] Zhu Y, Liao Y, Lu L, Lv W, Liu J, Song X, et al. Oxidative Catalytic Fractionation of Lignocellulose to High-Yield Aromatic Aldehyde Monomers and Pure Cellulose. ACS Catal. 2023 June 16;13(12):7929–41.

[24] Bhatu MN, Malvankar GR, Chavan A, Baikar PP, Raut DS, Patil SP. Eco-Friendly Fabrication of Ag-Ni Bimetallic Nanocatalyst for Catalytic Reduction of 4-Nitrophenol and Photodegradation of Crystal Violet Dye with Antibacterial Applications. Iran J Catal [Internet]. 2026 [cited 2025 Dec 23];16(01). Available from: https://oiccpress.com/ijc/article/view/18144

[25] Dudhani S, Mavlankar G, Chavan A, Aade D, Patil S. Mitigating Sublime Nature of Camphor via Pickering Emulsion Method for Sustained Antibacterial Efficacy. Int J Sci Res Sci Technol. 2024 Mar 1;11(11):106–17.

[26] Chavan A, Pawar J, Kakde U, Venkatachalam M, Fouillaud M, Dufossé L, et al. Pigments from Microorganisms: A Sustainable Alternative for Synthetic Food Coloring. Fermentation. 2025 July 10;11(7):395.

[27] Chavan A, Mavlankar G, Khan A, Mourya N, Salve A, Kakde U. Response Surface Methodology-Based Optimization of Natural Pigment Production from Penicillium purpurogenum. GSC Biol Pharm Sci. 2025 Dec 31;33(3):245–55.

[28] Chavan A, Pawar jaya, Kakde U. Fungal Pigment & its Potential in Nanoparticle Synthesis, Characterization and its Application. Adv Bioresearch. 2023 Sept;14(5):349–55.

[29] Segal L, Creely JJ, Martin AE, Conrad CM. An Empirical Method for Estimating the Degree of Crystallinity of Native Cellulose Using the X-Ray Diffractometer. Text Res J. 1959 Oct;29(10):786–94.

[30] Iglesias MC, Shivyari N, Norris A, Martin-Sampedro R, Eugenio ME, Lahtinen P, et al. The effect of residual lignin on the rheological properties of cellulose nanofibril suspensions. J Wood Chem Technol. 2020 Nov 1;40(6):370–81.

[31] Cao C, Yang Z, Han L, Jiang X, Ji G. Study on in situ analysis of cellulose, hemicelluloses and lignin distribution linked to tissue structure of crop stalk internodal transverse section based on FTIR microspectroscopic imaging. Cellulose. 2015 Feb;22(1):139–49.

[32] De Castro DO, Bras J, Gandini A, Belgacem N. Surface grafting of cellulose nanocrystals with natural antimicrobial rosin mixture using a green process. Carbohydr Polym. 2016 Feb;137:1–8.

[33] Hynninen V, Mohammadi P, Wagermaier W, Hietala S, Linder MB, Ikkala O, et al. Methyl cellulose/cellulose nanocrystal nanocomposite fibers with high ductility. Eur Polym J. 2019 Mar;112:334–45.

[34] Oliveira JPD, Bruni GP, Lima KO, Halal SLME, Rosa GSD, Dias ARG, et al. Cellulose fibers extracted from rice and oat husks and their application in hydrogel. Food Chem. 2017 Apr;221:153–60.

[35] Bartos A, Anggono J, Farkas ÁE, Kun D, Soetaredjo FE, Móczó J, et al. Alkali treatment of lignocellulosic fibers extracted from sugarcane bagasse: Composition, structure, properties. Polym Test. 2020 Aug;88:106549.

[36] Isogai A, Saito T, Fukuzumi H. TEMPO-oxidized cellulose nanofibers. Nanoscale. 2011;3(1):71–85.

[37] Marchessault RH, Liang CY. Infrared spectra of crystalline polysaccharides. III. Mercerized cellulose. J Polym Sci. 1960 Mar;43(141):71–84.

[38] Geng H, Wang Y, Yu Q, Gu S, Zhou Y, Xu W, et al. Vanillin-Based Polyschiff Vitrimers: Reprocessability and Chemical Recyclability. ACS Sustain Chem Eng. 2018 Nov 5;6(11):15463–70.

[39] Ávila Ramírez JA, Suriano CJ, Cerrutti P, Foresti ML. Surface esterification of cellulose nanofibers by a simple organocatalytic methodology. Carbohydr Polym. 2014 Dec;114:416–23.

[40] Mavlankar GR, Baikar PP, Rangadal DN, Chavan A, Malkhede K, Bhatu MN, et al. Esterification of nanocellulose with ferulic acid: A sustainable approach towards robust antibacterial material. Carbohydr Res. 2026 Jan;559:109737.